



Construction of rBCG carrying the *IL-2-BZLF1* fusion gene and its immunological function

Meimei Yu^{1,2} · Tian Mi¹ · Jiaqi Lu¹ · Lixian Cui¹ · Qingjie Xue¹ · Huabao Xiong^{1,3} · Yinlong Li⁴

Received: 12 May 2023 / Revised: 22 September 2023 / Accepted: 3 October 2023
© The Author(s), under exclusive licence to Springer-Verlag GmbH Germany, part of Springer Nature 2024

Abstract

In this research, a recombinant *Bacillus Calmette Guerin* (rBCG) vector vaccine carrying a human *IL-2* and EBV *BZLF1* fusion gene (*IL-2-BZLF1*-rBCG) was constructed. The *IL-2-BZLF1*-rBCG construct was successfully generated and stably expressed the *IL-2* and *BZLF1* proteins. *IL-2-BZLF1*-rBCG activated the immune system and promoted the secretion of $\text{IFN-}\gamma$ and $\text{TNF-}\alpha$ by CD4^+ and CD8^+ T cells. *IL-2-BZLF1*-rBCG activated lymphocytes to effectively kill EBV-positive NPC cells *in vitro*. Additionally, *IL-2-BZLF1*-rBCG stimulated the proliferation of NK cells and lymphocytes *in vivo*, activated related immune responses, and effectively treated EBV-positive NPC. The immune response to and pharmacological effect of *IL-2-BZLF1*-rBCG were explored *in vitro* and *in vivo* to provide a theoretical and experimental basis for the prevention and treatment of EBV-positive tumors with an rBCG vector vaccine.

Key points

- rBCG with human *IL-2* and *BZLF1* of EB virus was constructed
- The *IL-2-BZLF1* fusion gene was stably expressed with rBCG
- rBCG with *IL-2-BZLF1* has an obvious immune response *in vitro* and *in vivo*

Keywords Epstein-Barr virus · *BZLF1* · *IL-2* · BCG · Tumor

Introduction

Epstein–Barr virus (EBV) is a γ herpesvirus that was initially isolated by Epstein and Barr in 1964 from malignant lymphoma samples from children in Africa. EBV is defined

as a class I carcinogen by the World Health Organization (Kanda et al. 2019). More than 95% of the world's population has been infected with EBV (Yin et al. 2019), but most people are latently infected (Kerr 2019) and do not experience any symptoms (Bernaudat et al. 2022). EBV is closely associated with the development of many cancers, such as Burkitt's lymphoma, Hodgkin's lymphoma, and nasopharyngeal carcinoma (Kanda et al. 2019), but there is no effective treatment for EBV-associated tumors. In addition, EBV has been associated with the development of systemic lupus erythematosus, multiple sclerosis, and rheumatoid arthritis (Hartlage et al. 2015).

EBV is a linear double-stranded DNA virus with a biphasic infection cycle, and it primarily infects lymphocytes and oropharyngeal epithelial cells. EBV infection includes two phases: the latent phase and the lytic phase. During the latent phase, EBV is not infectious, and the genome replicates with the host cell cycle in the form of nuclear appendages (Hartlage et al. 2015; Mizui 2019). EBV can express genes related to latency, such as EBNA_s, LMP_s, EBER_s, miRNAs, EBNA2 and EBNA_{LP}, as well as transcription factors that drive quiescent B lymphocytes to enter the cell cycle,

Meimei Yu, Tian Mi and Jiaqi Lu contributed equally to this work.

- ✉ Qingjie Xue
qjxue9797@mail.jnmc.edu.cn
- ✉ Huabao Xiong
huabao.Xiong@mssm.edu
- ✉ Yinlong Li
75294669@qq.com

- ¹ School of Basic Medical, Jining Medical University, Jining 272067, Shandong, China
- ² Laboratory Department, Qingdao Geriatric Hospital, Qingdao 266002, Shandong, China
- ³ Precision Immunology Institute, Icahn School of Medicine at Mount Sinai, New York, NY 10029, USA
- ⁴ School of Public Health, Jining Medical University, Jining 272067, China

promote B-cell growth and transformation, and cause cancer (Kanda et al. 2019). EBV persists in a latent state in the host for a long time and is not easily recognized by the immune system (Yan et al. 2020). The immediate early transcription factor Zta (BZLF1 protein), which is encoded by the EBV gene BZLF1, activates the transcription factor Rta, which is encoded by the gene BRLF1, and together, Zta and Rta activate EBV to transition from the latent phase to the lytic phase (Cui and Snapper 2021). During the lytic phase, EBV expresses more than 80 lysogenic proteins and promotes the production of infectious viral particles (Marques-Neto et al. 2021). During the lytic phase, EBV is readily recognized by the immune system and induces the death of already infected cells, which can also be used as a therapeutic strategy for EBV-associated tumors.

The EBV gene *BZLF1* encodes Zta (BZLF1 protein), which belongs to the basic leucine zipper (bZIP) family of transcripts, and its bZIP region includes a DNA-binding domain (DBD) and a dimerization structural domain. Zta response elements (ZREs), which include CpG-free activator protein 1 (AP-1)-like recognition elements and CpG-containing recognition elements, are highly methylated and transcriptionally repressed in the EBV genome during latency, and Zta activates gene transcription by binding to CpG-ZRE-containing methylated regions; Zta is highly immunogenic and stimulates adaptive immunity through CD4⁺ T cells and CD8⁺ T cells (Cui and Snapper 2021).

IL-2, which is a T-cell growth factor, is mainly produced by CD4⁺ T cells and to a lesser extent by CD8⁺ T cells and other cells (Rist et al. 2015). IL-2 is used by regulatory T cells (Tregs) to maintain the homeostasis of the immune system and to enhance the antitumor effects of the body by activating cytotoxic lymphocytes. In intrinsic immunity, IL-2 promotes the proliferation and differentiation of type II intrinsic lymphocytes and enhances the cytotoxic activity of NK cells and monocytes (Rist et al. 2015). With the identification and cloning of IL-2 and the advent of recombinant DNA technology (Salomon et al. 2018), research related to the use of IL-2 for tumor treatment has been ongoing since the 1980s. The antitumor effect of recombinant IL-2 has been reported to have a palliative effect on lung metastases and subcutaneous tumors (Raker et al. 2020). The safety and efficacy of BCG, which is one of the most widely used vaccines worldwide, are well documented. It has been reported that BCG exerts nonspecific protective effects against unrelated pathogens and can significantly reduce mortality in children (Xue et al. 2022). In recent years, BCG has been widely used to study vaccines against various pathogens, such as bacteria, viruses and parasites, because of its low toxicity as well as its safety and efficacy (Xue et al. 2022).

Given the complexity of the EBV infection cycle and the severity of EBV-positive tumors, we sought to develop an rBCG vector vaccine that is effective in the prevention and treatment of EBV-positive tumors. In this study, the human *IL-2* gene and EBV *BZLF1* gene were ligated to form a fusion gene by overlap extension PCR, and a recombinant plasmid was constructed by ligating this fusion gene with the *E. coli-Mycobacterium tuberculosis* shuttle expression vector pMV261. The plasmid was transformed into BCG to generate *IL-2-BZLF1*-rBCG, and the expression of the fusion construct was measured by Western blotting and qRT-PCR. Finally, this study explored the immune response induced by *IL-2-BZLF1*-rBCG in mice and the pharmacological effect of *IL-2-BZLF1*-rBCG on EBV-positive tumors in animal experiments to provide effective guidance for the prevention and treatment of EBV-positive tumors.

Materials and methods

Materials

The *IL-2* gene (GenBank: V00564.1) was synthesized by Sangon Biotech Co., Ltd. (Shanghai, China). The EBV gene *BZLF1* (GenBank: M17547.1), plasmid pMV261, *E. coli DH5α* and BCG Shanghai Denmark strain were preserved in our laboratory (Xue et al. 2022). The PCR mix, plasmid kit and agarose gel recovery kit were purchased from Tiangen Biotech Co. Ltd. (Beijing, China). *Sal* I, *Bam* H I, *Hind* III, *Eco* R I, T4 DNA ligase and DNA Marker were produced by TaKaRa Co., Ltd. (Dalian, China). The multicolor prestained protein ladder (10–180 kD) and HRP-labeled goat anti-rabbit IgG II antibody were obtained from Beyotime Biotech Co. Ltd. (Shanghai, China). C57BL/6 J mice and BALB/c-nu nude mice were purchased from Jinan Ponyue Laboratory Animal Breeding Co., Ltd. (Shanghai, China). All animal experiments were approved by the Shandong animal experimentation committees (2009–0023; approval date, 2/25/09–3/25/14). The anti-BZLF1 monoclonal antibody was purchased from Santa Cruz Biotechnology (Danvers, MA, USA). The anti-IL-2 monoclonal antibody was purchased from Affinity Biosciences (Shanghai, China). Mouse CD3 (PE), CD4 (FITC), CD8 (APC) and NK1.1 (PE) antibodies were purchased from Biolegend (Beijing, China). Difco™ Middlebrook 7H9 Broth, Difco™ Middlebrook 7H10 Agar, BBL™ Middlebrook ADC Enrichment and BBL™ Middlebrook OADC Enrichment were obtained from BD Co. Ltd. (Franklin, NJ, USA). The HiScript® III RT SuperMix for qPCR and AceQ® qPCR SYBR Green Master Mix were purchased from Nanjing Nuvisan Biotechnology Co., Ltd. (Nanjing, China). CNE-2Z cells (EB virus-positive cell line) were preserved in our laboratory.

Methods

Primer design and synthesis

Primers were designed based on known sequences, and the results were as follows. The *IL-2-F* sequence was 5'-GCGGGATCCGATGTACAGGATGCAACTCCTGTC-3'. The *IL-2-r* sequence was 5'-GCTGCCGCCACCGCCGCTTCCGCCACCGCCACCTCAAGTTAGTGTGAGATGATGC. The *IL-2-R* sequence was CGCAAGCTTTTATCAAGTTAGTGTGAGATGATGC. The *BZLF1-f* sequence was GGTGGCGGTGGAAGCGGC GGTGGCGGAAGCGGC GGTGGCGGCAGCATGATGACCCAAACTCGACTTCTG. The *BZLF1-R* sequence was GCGGTCTGACTAAGAAATTTAAGAGATCCTCGTG. The *BZLF1-F* sequence was GCGGTCTGACTAAGAAATTTAAGAGATCCTCGTG. Italics indicate endonuclease sequences, bold underline indicates linker sequences (Fig. 2A). The designed primers were synthesized by Bioengineering Co. (Shanghai, China). PCR amplification was performed using the *IL-2* gene as a template in a total volume of 50 μ l. PCR amplification was performed using the *BZLF1* gene as a template in a total volume of 50 μ l.

Enzymatic cleavage of the *IL-2* and *BZLF1* genes and the pMV261 plasmid

The PCR products were subjected to 1% agarose gel electrophoresis and agarose gel DNA recovery, and the agarose gel DNA recovery steps were performed according to the instructions of the kit (Tiangen Biotech, Beijing, China). The *IL-2* gene product that was recovered from the gel was digested simultaneously with the plasmid pMV261 (Fig. 2B) by *Hind* III, and the digestion reaction included 10 μ l of template, 1 μ l of *Hind* III, 2 μ l of 10 \times M buffer and 7 μ l of ddH₂O. The components were completely mixed, and the reaction was incubated in a water bath at 37 $^{\circ}$ C overnight. The *BZLF1* gene product that was recovered from the gel was digested simultaneously with the plasmid pMV261 by *Sal* I, and the digestion reaction included 10 μ l of template, 1 μ l of *Sal* I, 2 μ l of 10 \times M buffer and 7 μ l of ddH₂O. The components were completely mixed, and the reaction was incubated in a water bath at 37 $^{\circ}$ C overnight.

Conversion of *IL-2*-pMV and *BZLF1*-pMV

The *IL-2*-pMV conjugate and *BZLF1*-pMV conjugate were mixed with *E. coli DH5 α* receptor cells (removed from the freezer in advance and thawed on ice), and the mixture was incubated in an ice bath for 30 min. Then, the cells were heat shocked at 42 $^{\circ}$ C for 90 s and incubated in an ice bath for 10

min. Then, 800 μ l LB liquid medium was added and mixed well, and the culture was mixed at 160 rpm at 37 $^{\circ}$ C for 1 h. Then, the cells were centrifuged at 5000 rpm for 3 min, and approximately 700 μ l of the supernatant was discarded. The remaining supernatant was mixed, the cells were plated on LB solid medium containing Kan^r, and the plates were incubated for 18–24 h at 37 $^{\circ}$ C in an incubator.

Single colonies of *E. coli DH5 α* carrying *IL-2*-pMV or *BZLF1*-pMV were picked as follows. Single colonies were picked from LB solid medium (supplemented with kan, 50 μ g/ml) and inoculated into 5 ml LB liquid medium using a splicing ring. Then, 5 μ l of 50 mg/ml kanamycin was added to the medium, and the bacteria were incubated for 12–18 h at 37 $^{\circ}$ C in a shaker at 160 rpm.

PCR identification of the recombinant plasmids *IL-2*-pMV and *BZLF1*-pMV

The recombinant plasmids *IL-2*-pMV and *BZLF1*-pMV were used as templates for PCR identification, and the total PCR volume was 25 μ l. The amplification reaction included 0.5 μ l of the recombinant plasmid *IL-2*-pMV, 0.2 μ l of the primer *IL-2-F*, 0.2 μ l of the primer *IL-2-R*, 5 μ l of 5 \times PrimeSTAR GXL buffer, 2 μ l of dNTP mixture and 0.5 μ l of PrimeSTAR GXL DNA polymerase. After adding 16.6 μ l ddH₂O, the components were completely mixed. The following reaction conditions were used: predenaturation at 98 $^{\circ}$ C for 4 min; 30 cycles of denaturation at 98 $^{\circ}$ C for 10 s, annealing at 60 $^{\circ}$ C for 15 s and extension at 68 $^{\circ}$ C for 30 s; and extension at 68 $^{\circ}$ C for 5 min.

The amplification reaction included 0.5 μ l of the recombinant plasmid *BZLF1*-pMV, 0.2 μ l of the primer *BZLF1-F*, 0.2 μ l of the primer *BZLF1-R*, 5 μ l of 5 \times PrimeSTAR GXL Buffer, 2 μ l of dNTP mixture and 0.5 μ l of PrimeSTAR GXL DNA polymerase. After adding 16.6 μ l ddH₂O, the components were completely mixed. The following reaction conditions were used: predenaturation at 98 $^{\circ}$ C for 4 min; 30 cycles of denaturation at 98 $^{\circ}$ C for 10 s, annealing at 60 $^{\circ}$ C for 15 s, and extension at 68 $^{\circ}$ C for 1 min; and extension at 68 $^{\circ}$ C for 5 min.

Identification of *IL-2*-pMV and *BZLF1*-pMV

The recombinant plasmid *IL-2*-pMV was digested with *Bam*H I and *Hind* III. The total volume was 20 μ l, and the digestion reaction included 10 μ l of *IL-2*-pMV, 1 μ l of *Bam*H I, 1 μ l of *Hind* III, 2 μ l of 10 \times K buffer and 6 μ l of ddH₂O. The components were completely mixed, and the mixture was incubated in a water bath at 30 $^{\circ}$ C overnight. *BZLF1*-pMV was digested with *Bam*H I and *Sal* I. The total volume was 20 μ l, and the digestion reaction included 10 μ l of *BZLF1*-pMV, 1 μ l of *Bam*H I, 1 μ l of *Sal*I, 2 μ l of 10 \times K buffer and 6 μ l of ddH₂O. The

components were completely mixed, and the mixture was incubated in a water bath at 30 °C overnight. The PCR products of *IL-2*-pMV and *BZLF1*-pMV and the two products of double-enzyme digestion were subjected to 1% agarose gel electrophoresis. The *IL-2*-pMV and *BZLF1*-pMV PCR and restriction digestion products were sent to Bioengineering Co., Ltd. (Shanghai, China) for gene sequencing.

Construction of the recombinant plasmid *IL-2-BZLF1*-pMV

The fusion gene construction method is shown in Fig. 1A. The products of *IL-2-BZLF1* and pMV261 that were recovered from the gel in the previous step were ligated with T4 DNA ligase, and the following ligation reaction conditions were used: 20 µl of the *IL-2-BZLF1* gel recovery product, 20 µl of the pMV261 gel recovery product, 5 µl of T4 DNA ligase and 5 µl of 10×T4 buffer. The components were then completely mixed and incubated at 16 °C overnight.

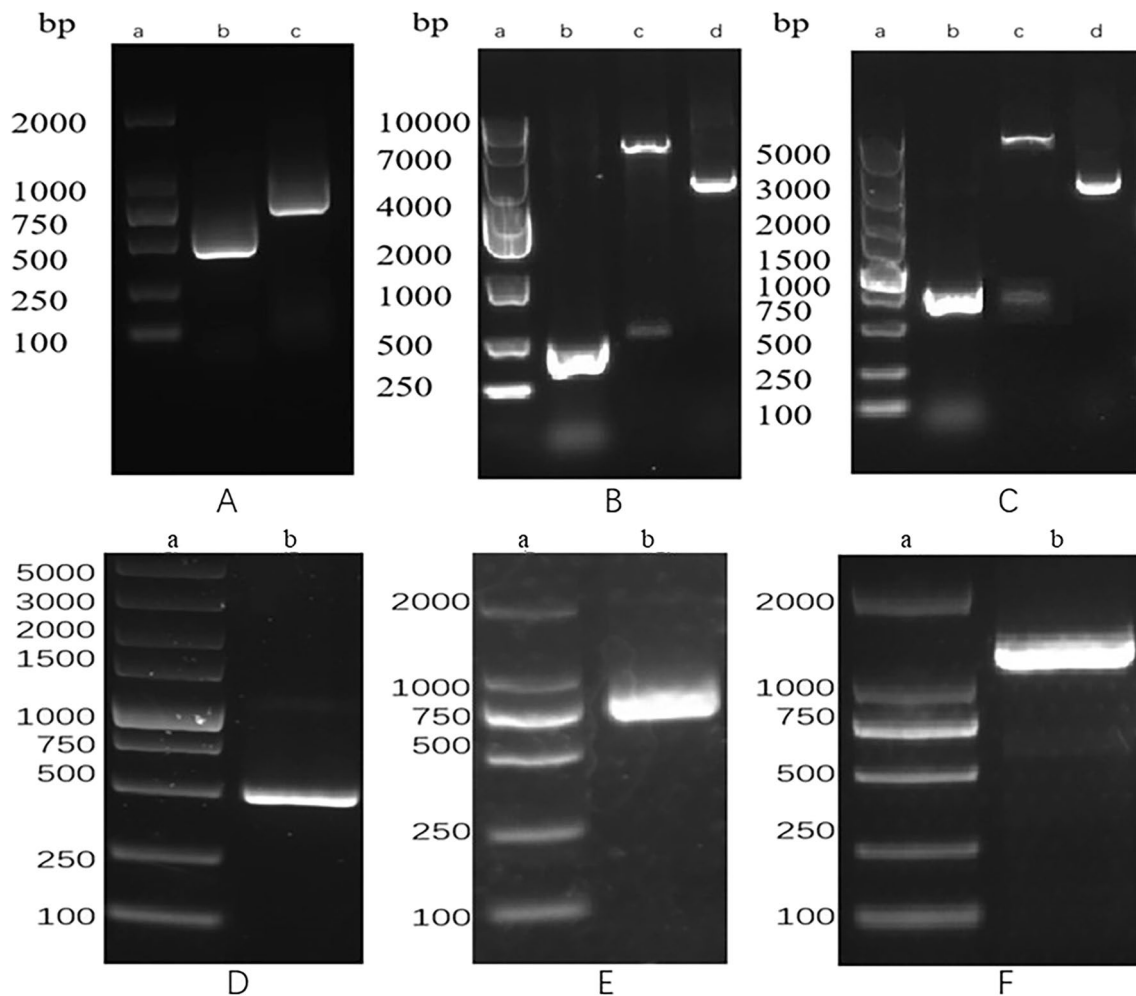


Fig. 1 Identification of the recombinant plasmids *IL-2*-pMV, *BZLF1*-pMV and *IL-2-BZLF1*-pMV with PCR and restriction enzyme digestion. **A** Results of PCR amplification of the *IL-2* and *BZLF1* genes; (a) DNA Marker DL (2000); (b) products of PCR amplification of the *IL-2* gene; (c) products of PCR amplification of the *BZLF1* gene. **B** Results of identification of recombinant plasmid *IL-2*-pMV; (a) DNA Marker DL (10,000); (b) PCR Identification of recombinant plasmid *IL-2*-pMV; (c) Double restriction enzyme digestion of recombinant plasmid *IL-2*-pMV; (d) Agarose gel electrophoresis of recombinant plasmid *IL-2*-pMV; **C** Results of identification of recombinant plasmid *BZLF1*-pMV; (a) DNA Marker DL (5000); (b) PCR identifica-

tion of recombinant plasmid *BZLF1*-pMV; (c) The result of restriction enzyme digestion of recombinant plasmid *BZLF1*-pMV; (d) The result of agarose gel electrophoresis of recombinant plasmid *BZLF1*-pMV; **D** Results of agarose gel electrophoresis of *IL-2* gene PCR amplification product. (a) DNA marker DL (5000); (b) *IL-2* gene PCR amplification product. **E** Results of agarose gel electrophoresis of the *BZLF1* gene PCR amplification product. (a) DNA marker DL (2000); (b) *BZLF1* gene PCR amplification product. **F** Results of agarose gel electrophoresis of the *IL-2-BZLF1* gene PCR amplification product. (a) DNA marker DL (2000); (b) *IL-2-BZLF1* was amplified by overlap extension PCR

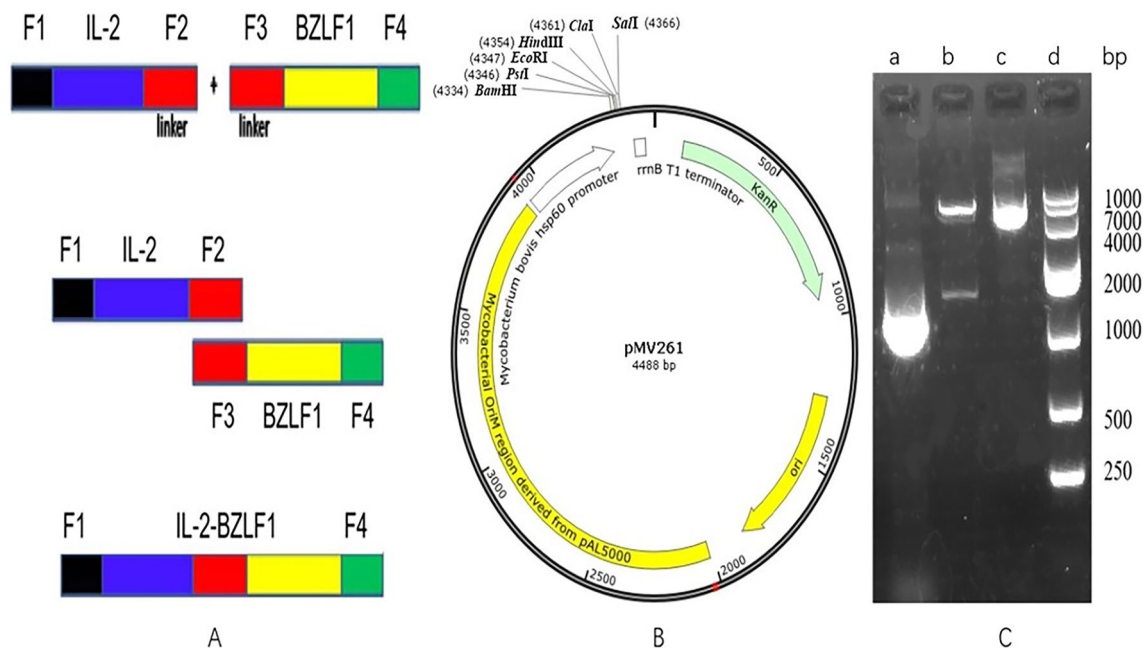


Fig. 2 Construction of rBCG. **A** Schematic of fusion gene synthesis. **B** pMV261 plasmid. **C** Agarose gel electrophoresis results for identification. (a) PCR identification results of the *IL-2-BZLF1* gene; (b)

double digestion identification results of *IL-2-BZLF1*-pMV; (c) agarose gel electrophoresis of the recombinant plasmid *IL-2-BZLF1*; (d) DNA marker DL(10,000)

IL-2-BZLF1-pMV was constructed as previously described (Yan et al. 2020). The recombinant plasmid *IL-2-BZLF1*-pMV, the PCR product and the double-enzyme digestion products were simultaneously subjected to 1% agarose gel electrophoresis. After confirmation by PCR and digestion, the *IL-2-BZLF1*-pMV product was sent to Bioengineering Co., Ltd. (Shanghai) for gene sequencing.

Culture and identification of rBCG

BCG competent cells were incubated in a shaker for 24 h at 37 °C and 160 rpm. The rotor cup was rinsed repeatedly with ddH₂O, soaked in 75% alcohol for 10 min, dried and stored at -20 °C. The next day, the electroporated rBCG sample was removed from the shaker and centrifuged at 5000 rpm for 10 min, and 900 µl of the supernatant was removed. The remaining supernatant was mixed with the cells, and the cells were plated on Middlebrook 7H10 solid medium supplemented with 50 µg/ml kanamycin and cultured in a 37 °C incubator for 3–4 weeks.

A single colony was picked from Middlebrook 7H10 solid medium and inoculated into 100 ml Middlebrook 7H9 liquid medium (BD Co., Ltd., Franklin, NJ, USA) supplemented with 50 µg/ml kanamycin, and the cells were cultured until they reached the logarithmic growth phase. Small aliquots of *IL-2-BZLF1*-rBCG, *IL-2*-rBCG and *BZLF1*-rBCG bacteria that had reached the logarithmic growth phase were used for acid-fast staining.

Expression and identification of fusion proteins

The absorbance of *IL-2-BZLF1*-rBCG, *IL-2*-rBCG and *BZLF1*-rBCG bacteria that had reached the logarithmic growth phase was measured, and the concentration was adjusted to OD₆₀₀ = 0.6; then, 2 ml of bacterial broth was incubated on a 45 °C shaker at 160 rpm for 45 min to induce protein expression (Xue et al. 2022). The cells were incubated under these induction conditions for 3 days, and after induction, they were centrifuged at 12,000 rpm for 1 min.

A total of 1 ml of PBS was used to wash the cell pellet, and the cells were centrifuged at 12,000 rpm for 1 min; these wash steps were repeated once. Then, 100 µl of protein lysis buffer was added, and the mixture was incubated in an ice bath for 30 min. The centrifuge tube was placed on ice for sonication. The ultrasound settings were as follows: power of 300 W, working time of 10 s, rest time of 15 s, and cycle time of 30 min. Then, the samples were centrifuged at 12,000 rpm at 4 °C for 30 min, 80 µl of the supernatants were transferred to new centrifuge tubes, 20 µl of SDS–PAGE protein loading buffer (5×) was added, and the samples were mixed well. The samples were boiled in a metal bath at 99 °C for 10 min and stored at -20 °C.

BCG and rBCG were lysed with an ultrasonic breaker and separated by 12% SDS–PAGE. A BZLF1 antibody and IL-2 antibody were used to probe the proteins of interest, and the secondary antibodies that were used were goat anti-mouse antibodies. ECL chemiluminescence kits were

used to observe and analyze the results. A Chemi Doc MP Imaging System (Bio-Rad) was used to scan and analyze the protein bands.

Reverse transcription of rBCG

RNA was extracted from rBCG. Then, genomic DNA was removed; the total volume was 16 μ l, and the reaction included 8 μ l of template RNA, 4 μ l of 4 \times gDNA wiper mix and 4 μ l of RNase-free ddH₂O. The components were evenly mixed and incubated at 42 °C for 2 min. Reverse transcription was performed with the solution of the previous step in a total volume of 20 μ l. The reaction included 16 μ l of the reaction solution from the previous step and 4 μ l of 5 \times HiScriptIII qRT SuperMix. After mixing the solution, the reverse transcription reaction was carried out, and the specific reaction conditions were incubation at 37 °C for 15 min and 85 °C for 5 min.

qRT–PCR analysis of rBCG

The BCG-qF sequence was 5'-GGAGGCAGCAGTGGG GAATA-3'. The BCG-qR sequence was TCGTTCGATG GTGAAAGAGGTTTA. The *IL-2*-qF sequence was TCC CAAACTCACCAGGATGC. The *IL-2*-qR sequence was CGTTGATATTGCTGATTAAGTCCCT. The *BZLF1*-qF sequence was AAATTTAAGAGATCCTCGTGTAACATC. The *BZLF1*-qR sequence was CGCCTCCTGTTG AAGCAGAT. The designed primers were synthesized by Bioengineering (Shanghai) Co., Ltd.

qRT–PCR was carried out using the cDNA product as the template, and the total volume was 20 μ l. The reaction system included 0.5 μ l of template cDNA, 0.5 μ l of Primer qF, 0.5 μ l of Primer qR, 10 μ l of 2 \times AceQ qPCR SYBR Green and 8.5 μ l of ddH₂O. After mixing the system, real-time quantitative PCR was carried out. The specific reaction conditions were as follows: 95 °C for 5 min for 1 cycle; 95 °C for 10 s, 60 °C for 30 s, and 72 °C for 30 s for 45 cycles with fluorescence read at 72 °C; followed by 95 °C for 15 s, 60 °C for 60 s, and 95 °C for 15 s for 1 cycle.

Animal immunization and in vitro killing experiments with rBCG

C57BL/6J mice were purchased from Jinan Pengyue Experimental Animal Breeding Co., Ltd. (Jinan, China). Female C57BL/6J mice at 6–8 weeks of age with similar body weights were randomly divided into 5 groups: the PBS group, BCG group, *IL-2*-rBCG group, *BZLF1*-rBCG group and *IL-2* group-*BZLF1*-rBCG group.

Immunization with rBCG

A small amount of BCG, *IL-2*-rBCG, *BZLF1*-rBCG and *IL-2*-*BZLF1*-rBCG was harvested at the linear growth phase and centrifuged at 12,000 rpm for 1 min. The supernatants were removed, 1 ml of PBS was added to wash the cells, the absorbance of rBCG was adjusted to OD₆₀₀=2.1 (approximately 10⁷/ml cells with a Petrof Hausser bacterial count board (Treuer and Haydel 2011)) with PBS, and 100 μ l was injected intraperitoneally per mouse. Three injections were given every two weeks (Xue et al. 2022).

Isolation of lymphocytes

Two weeks after the last injection, blood was collected from the retro-orbital sinus of the mice and transferred to a heparin anticoagulation tube, and the spleens of the mice were harvested. The blood samples were allowed to stand for 15 min and were centrifuged at 3500 rpm at 4 °C for 15 min. The upper plasma layers were transferred to new centrifuge tubes, and 1 ml of erythrocyte lysis buffer was added to the blood cell pellets. The solutions were mixed well and transferred to 15 ml centrifuge tubes. Next, 4 ml of erythrocyte lysis buffer was added, and the samples were mixed well and allowed to stand for 5 min. Then, 8 ml of PBS was added, and the samples were mixed well and centrifuged at 1500 rpm for 5 min; then, the supernatants were removed. This step was repeated until the red blood cells were completely lysed. The spleens were homogenized in PBS; all the cells were transferred to a centrifuge tube after homogenization and centrifuged at 1500 rpm for 5 min. Then, the supernatants were removed. A total of 3 ml of erythrocyte lysis buffer was added, and the samples were mixed and allowed to stand for 5 min. Then, 10 ml of PBS was added, the samples were centrifuged at 1500 rpm for 5 min, and the supernatants were removed. This process was repeated until the red blood cells were completely lysed. After complete red blood cell lysis, the blood lymphocytes and splenic lymphocytes were filtered through a filter to obtain blood lymphocytes and splenic lymphocytes.

Flow cytometry analysis of cytokine expression by T cells

The blood lymphocytes and splenic lymphocytes were centrifuged at 1500 rpm for 5 min, and the supernatants were removed. A total of 1 ml of 1640 complete medium was added to wash the cells, and the cells were centrifuged at 1500 rpm for 5 min. The supernatants were removed, and the cells were resuspended in 1 ml of 1640 complete medium. Then, 0.2 μ l PMA, 2 μ l ionomycin and 1 μ l monensin were added and mixed well, and the samples were incubated at 37 °C for 4–6 h. The cells were collected by centrifugation

at 1500 rpm for 5 min, the supernatants were removed, 1 ml of PBS was added and mixed well, the cells were centrifuged again at 1500 rpm for 5 min, and the supernatants were removed. Then, 100 μ l PBS was added and mixed well, 0.25 μ l mouse anti-CD4 flow antibody (FITC) and mouse anti-CD8 flow antibody (APC) were added and mixed well, and the samples were incubated at 4 °C for 30 min in the dark. Then, 1 ml of PBS was added to wash the cells, and the cells were centrifuged at 1500 rpm for 5 min to remove the supernatants; these washing steps were repeated once. Then, 800 μ l IC fixation buffer was added and mixed well, and the samples were incubated at 4 °C for 30 min in the dark. The samples were centrifuged at 1500 rpm for 5 min, 1 ml of PBS was added, and the samples were centrifuged at 1500 rpm for 5 min to remove the supernatants. Then, 1 ml of 1 \times permeabilization buffer was added and mixed well, and the cells were centrifuged at 1500 rpm for 5 min to remove the supernatants. Then, 100 μ l 1 \times permeabilization buffer, 0.25 μ l mouse anti-IFN- γ flow antibody (PE) and mouse anti-TNF- α flow antibody (V450) were added, mixed well, and incubated overnight at 4 °C in the dark. The next day, 1 ml of PBS was added to wash the cells, the cells were centrifuged at 1500 rpm for 5 min, and then, the supernatants were removed. A total of 200 μ l PBS was added to resuspend the cells, the cells were filtered, and flow cytometry analysis was performed.

In vitro stimulation of splenic lymphocytes by rBCG

Splenic lymphocytes from 6 randomly selected mice were centrifuged at 1500 rpm for 5 min, washed with 1 ml of 1640 complete medium, and centrifuged at 1500 rpm for 5 min. The cells were quantitatively divided into 3 portions and plated in a 48-well plate, and the volume was adjusted to 1 ml with 1640 complete medium. Then, 100 μ l PBS was added to the PBS group; 100 μ l PBS, 10³/ml BCG or 10⁶/ml BCG was added to the BCG group; 100 μ l PBS, 10³/ml *IL-2*-rBCG or 10⁶/ml *IL-2*-rBCG was added to the *IL-2*-rBCG group; 100 μ l PBS, 10³/ml *BZLF1*-rBCG or 10⁶/ml *BZLF1*-rBCG was added to the *BZLF1*-rBCG group; and 100 μ l PBS, 10³/ml *IL-2*-*BZLF1*-rBCG or 10⁶/ml *IL-2*-*BZLF1*-rBCG was added to the *IL-2*-*BZLF1*-rBCG group. The groups were cultured in a CO₂ incubator for 48 h.

Flow cytometry analysis of T-cell intracellular factors

Splenic lymphocytes were collected and centrifuged at 1500 rpm for 5 min, and the supernatants were removed. Then, 1 ml of 1640 complete medium was added and mixed well. Then, 0.2 μ l PMA, 2 μ l ionomycin and 1 μ l monensin were added and mixed well, and the cells were incubated at 37 °C for 4–6 h. The cells were collected by centrifugation at 1500

rpm for 5 min, and the supernatants were removed. A total of 1 ml of PBS was added and mixed, the cells were centrifuged at 1500 rpm for 5 min, and the supernatants were removed. A total of 100 μ l PBS was added and mixed, 0.25 μ l mouse anti-CD4 flow antibody (FITC) and mouse anti-CD8 flow antibody (APC) were added and mixed well, and the cells were incubated at 4 °C for 30 min in the dark. A total of 1 ml of PBS was added to wash the cells, and the cells were centrifuged at 1500 rpm for 5 min to remove the supernatants. These washing steps were repeated once. The samples were centrifuged at 1500 rpm for 5 min, 1 ml of PBS was added, and the samples were centrifuged at 1500 rpm for 5 min to remove the supernatants. A total of 1 ml 1 \times permeabilization buffer was added and mixed well, and the cells were centrifuged at 1500 rpm for 5 min to remove the supernatants. Then, 100 μ l 1 \times permeabilization buffer, 0.25 μ l mouse anti-IFN- γ flow antibody (PE) and mouse anti-TNF- α flow antibody (V450) were added, mixed well, and incubated overnight at 4 °C in the dark. The next day, 1 ml of PBS was added to wash the cells, and they were centrifuged at 1500 rpm for 5 min. Then, the supernatants were removed. A total of 200 μ l PBS was added to resuspend the cells, the cells were filtered, and flow cytometry analysis was performed.

Assessment of rBCG-specific lymphocyte killing efficiency

CNE-2Z cells were cultured in 1640 complete medium at 37 °C in CO₂. The cells were centrifuged at 1000 rpm for 5 min, the supernatants were removed, and 10 ml of 1640 complete medium was added and mixed. A 20 μ l cell suspension was used to measure the cell concentration, and the cell suspension was divided into 96-well plates in a volume of 100 μ l per well. Splenic lymphocytes from mice in the different immunization groups were added at CNE-2Z cell:splenic lymphocyte ratios of 1:1, 1:2 and 1:4, and the cells were cultured in a CO₂ incubator for 24 h. The lymphocytes and culture medium were aspirated, and 100 μ l PBS was added for washing. A total of 100 μ l of 1640 complete medium and 100 μ l of Cell Titer-Lumi TM Steady Plus luminescence cell viability detection reagent were added, and the samples were mixed at room temperature for 2 min to promote cell lysis. The mixture was incubated for 10 min at room temperature to stabilize the luminescence signal. The cells were placed into a microplate reader, and chemiluminescence was determined according to the formula $R = (X - Y) / X \times 100\%$, where R is the killing efficiency, X is the previous luminescence intensity of the CNE-2Z cells, and Y is the next luminescence intensity of the CNE-2Z cells. The luminescence intensity of CNE-2Z cells was used to calculate the ability of splenic lymphocytes to lyse CNE-2Z cells.

Treatment of EBV-positive tumors in animals

Experimental materials: BALB/c-nu nude mice were purchased from Jinan Pengyue Experimental Animal Breeding Co., Ltd. (Jinan, China). Twenty-five female BALB/c-nu nude mice of similar body weight were injected with 150 μ l CNE-2Z cells (at a concentration of 1.75×10^7 /ml), and the changes in tumor volume were measured and recorded daily.

rBCG injection

Twenty-five female BALB/c-nu nude mice in which NPC tumors were successfully established were randomly divided into 5 groups: the PBS group, BCG group, *IL-2*-rBCG group, *BZLF1*-rBCG group and *IL-2-BZLF1*-rBCG group. Bacterial counts were performed to prepare the following injections: 100 μ l of PBS, BCG (9×10^6 /ml), *IL-2*-rBCG (9×10^6 /ml), *BZLF1*-rBCG (9×10^6 /ml) and *IL-2-BZLF1*-rBCG (9×10^6 /ml) were administered to different parts of the tumors via infiltration injection, and injections were delivered once every 7 days for a total of 3 injections (Xue et al. 2022). Tumor volumes were measured every three days and recorded.

Tumor isolation and HE staining

Seven days after the last infiltration injection, the nude mice were sacrificed, and the tumors were removed, weighed and recorded. Additionally, the tumors were fixed with 4% paraformaldehyde and sent to Jinan Jinyu Co., Ltd. (Jinan, China) for HE staining to observe lymphocyte infiltration into the tumor tissues.

Flow analysis of NK cells

Seven days after the last infiltration injection, the nude mice were sacrificed, and the spleens were harvested. The spleens were placed in PBS for homogenization, filtered with a membrane, transferred into a centrifuge tube, and centrifuged at 1500 rpm for 5 min; then, the supernatants were removed. A total of 3 ml of red blood cell lysis buffer was added and mixed well, and the samples were allowed to stand at room temperature for 5 min. A volume of 9 ml of PBS was added to resuspend the cells, and the cells were centrifuged at 1500 rpm for 5 min to remove the supernatants. This process was repeated until the red blood cells were completely lysed. A total of 100 μ l PBS was added to resuspend the cells, 0.25 μ l mouse anti-NK1.1 flow antibody (PE) was added and mixed well, and the cells were incubated at 4 °C for 30 min in the dark. A volume of 1 ml of PBS was added to resuspend the cells, the cells were centrifuged at

1500 rpm for 5 min, and the supernatants were removed. This step was repeated, and the cells were resuspended in 200 μ l PBS for flow cytometry analysis.

Statistical analysis

GraphPad Prism 8.0 was used for the statistical analysis of the experimental data (expressed as the mean \pm SEM) that fit the normal distribution. In the flow analysis of rBCG-immunized mice, the assessment of the ability of rBCG-specific lymphocytes to kill EBV-positive cells in vitro, and the flow analysis of rBCG-treated EBV-positive nude mice, pairwise comparisons were performed using a paired *T* test, and one-way ANOVA was used between groups. If $P < 0.05$, the difference was considered statistically significant.

Results

Construction of *IL-2*-PMV, *BZLF1*-pMV and *IL-2-BZLF1*-pMV

After PCR amplification using *IL-2* and *BZLF1* as templates, bands with sizes of approximately 460 bp and 740 bp, respectively, were observed, and these bands were consistent with the expected sizes (Fig. 1A and Fig. S1A). The identities of *IL-2*-pMV and *BZLF1*-pMV were confirmed by PCR and double digestion, and the PCR and double digestion products of *IL-2*-pMV and *BZLF1*-pMV were subjected to 1% agarose gel electrophoresis. The electrophoresis results of *IL-2*-pMV showed that the PCR band was approximately 460 bp in size, and two bands of approximately 460 bp and 4500 bp appeared simultaneously after double digestion (Fig. 1B and Fig. S1B). The electrophoresis results of *BZLF1*-pMV showed that the PCR band was approximately 740 bp in size, and two bands of approximately 740 bp and 4500 bp appeared simultaneously after double digestion (Fig. 1C and Fig. S1C). The results of the identification of the two recombinant plasmids were consistent with expectations.

After PCR amplification of the *IL-2* and *BZLF1* genes, the products showed bands of approximately 460 bp (Fig. 1D and Fig. S1D) and 740 bp (Fig. 1E and Fig. S1E) in size, respectively, according to agarose gel electrophoresis, and these bands were consistent with the expected sizes. The agarose gel electrophoresis results of *IL-2-BZLF1* gene PCR amplification showed a product that was 1200 bp in size (Fig. 1F and Fig. S1F).

Identification of *IL-2-BZLF1*-pMV

The recombinant plasmid *IL-2-BZLF1*-pMV was used as the template for PCR and double digestion, and the PCR

and double digestion products were subjected to agarose gel electrophoresis together with the recombinant plasmid *IL-2-BZLF1*-pMV. The results showed a band of approximately 1200 bp after PCR and bands of 1200 bp and approximately 4500 bp after double digestion, which were consistent with the expected results (Fig. 2C and Fig. S2C).

Identification of rBCG

IL-2-BZLF1-rBCG, *IL-2*-rBCG and *BZLF1*-rBCG were cultured until they reached the logarithmic growth phase. Then, the cells were subjected to acid-fast staining, and the bacteria were stained red, morphologically rod-shaped and present in clusters according to oil microscopy. Therefore, all three rBCG strains (with 50 µg/ml kanamycin) were positive for acid-fast staining.

The proteins of the *IL-2-BZLF1*-rBCG, *IL-2*-rBCG and *BZLF1*-rBCG bacterial cultures, which were in the logarithmic growth phase, were extracted, and the proteins were subjected to Western blotting to measure the expression of the target proteins; the rBCG and BCG strains were used as blank controls. The results showed that *IL-2-BZLF1*-rBCG could express both the *IL-2* and *BZLF1* proteins with a size of approximately 55 kDa, *IL-2*-rBCG could express

the *IL-2* protein with a size of approximately 17 kDa, and *BZLF1*-rBCG could express the *BZLF1* protein with a size of approximately 38 kDa. All of these results were consistent with the expected results (Fig. 3A, B, C, D and Fig. S3A, S3B, S3C, S3D).

Real-time fluorescence quantitative PCR

RNA was extracted from *IL-2-BZLF1*-rBCG, *IL-2*-rBCG and *BZLF1*-rBCG cultures in the logarithmic growth phase and reverse transcribed into cDNA. Then, real-time fluorescence quantitative PCR was performed using cDNA as a template. The results showed that *IL-2* expression was upregulated in the *IL-2*-rBCG and *IL-2-BZLF1*-rBCG cultures ($P=0.0043$ and $P=0.0004$), and *BZLF1* expression was upregulated in the *BZLF1*-rBCG and *IL-2-BZLF1*-rBCG cultures ($P=0.0404$, $P=0.0063$) (Fig. 4).

Flow cytometry analysis of cytokine secretion by T cells stimulated with rBCG

Lymphocytes were isolated from the blood of rBCG-treated mice, and the expression of IFN- γ and TNF- α by CD4⁺ T cells and CD8⁺ T cells in different immunization groups

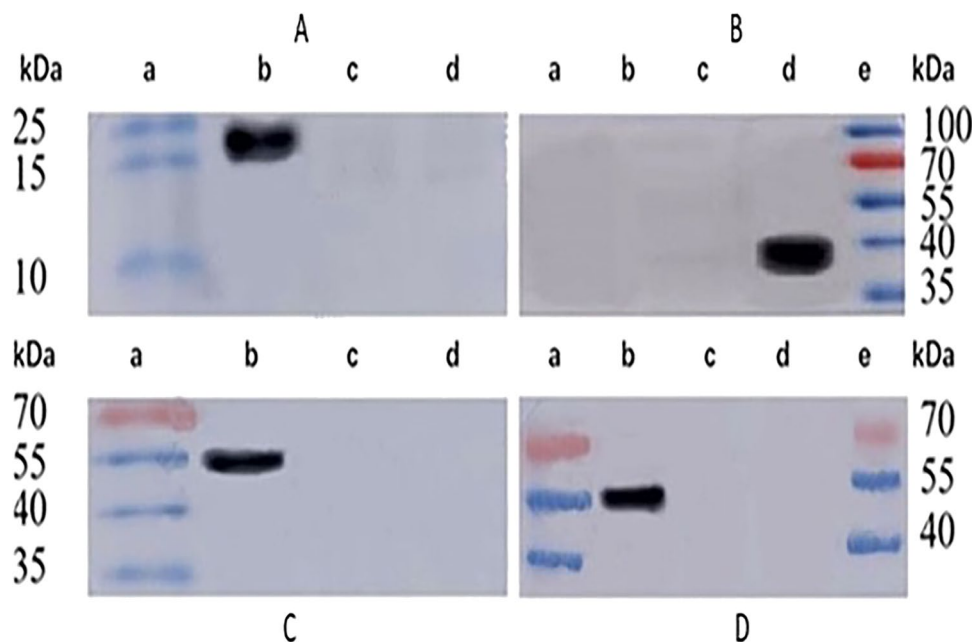


Fig. 3 Western blot results of rBCG. **A** Western blot results of *IL-2*-rBCG; (a) Protein molecular weight standard; (b) Detection of *IL-2* in rBCG; (c) Detection of *IL-2* in pMV261-BCG; (d) *IL-2* was detected in BCG. **B** Western blot results of *BZLF1*-rBCG; (a, b) Detection of *BZLF1* in BCG; (c) Detection of *BZLF1* in pMV261-BCG; (d) *BZLF1* was detected in *BZLF1*-rBCG; (e) Protein molecular weight standard. **C** Western blot results of *IL-2-BZLF1*-rBCG (primary antibody using *IL-2* antibody); (a) Protein molecular weight

standard; (b) *IL-2* detection in *IL-2-BZLF1*-rBCG; (c) *IL-2* detection in pMV261-BCG; (d) *IL-2* detection in BCG. **D** Western blot results of *IL-2-BZLF1*-rBCG (primary antibody using *BZLF1* antibody); (a) Protein molecular weight standard; (b) *BZLF1* detection in *IL-2-BZLF1*-rBCG; (c) *BZLF1* detection in pMV261-BCG; (d) *BZLF1* detection in BCG; (e) Protein molecular weight standard. (Notes: the concentration of *IL-2* mouse monoclonal antibody is 0.5 µg/ml and the concentration of *BZLF1* mouse monoclonal antibody is 1 µg/ml)

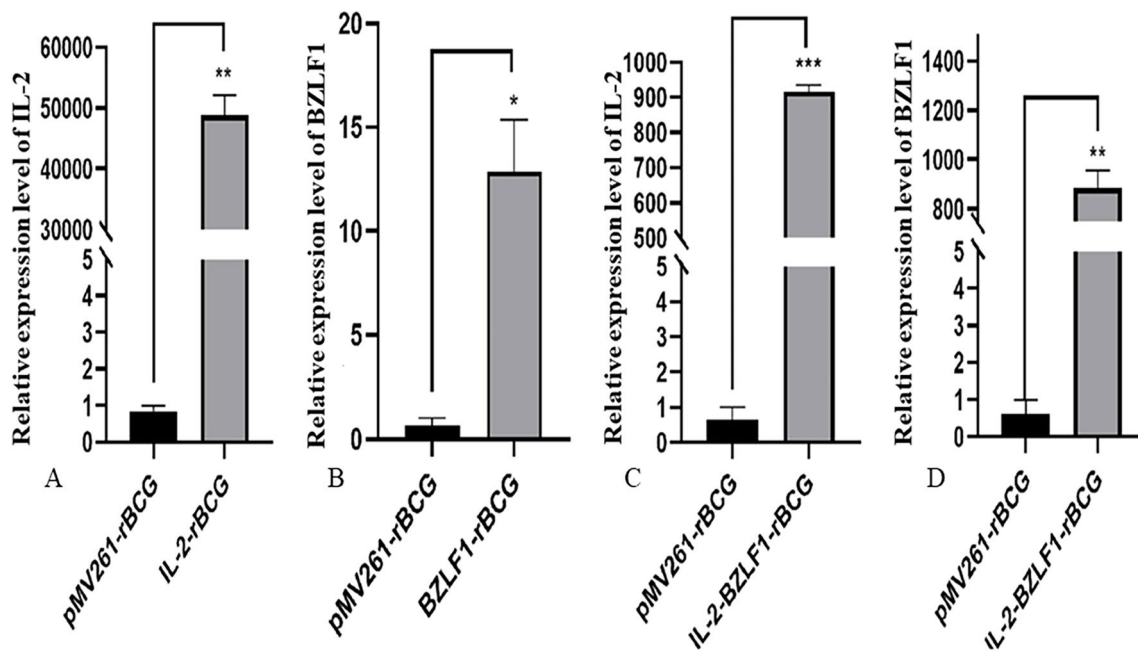


Fig. 4 Expression level of genes related to rBCG. **A** IL-2-related expression level in *IL-2*-rBCG. **B** BZLF1-related expression level in *BZLF1*-rBCG. **C** IL-2-related expression level in *IL-2-BZLF1*-rBCG. **D** *IL-2-BZLF1*-rBCG-related expression level in *BZLF1*-

rBCG; *: compared with pMV261-rBCG ($P < 0.05$); **: compared with pMV261-rBCG ($P < 0.01$); ***: compared with pMV261-rBCG ($P < 0.001$)

was analyzed by flow cytometry. The results showed that after *IL-2-BZLF1*-rBCG treatment, 1.21% of $CD4^+$ T cells secreted IFN- γ and 2.14% of $CD4^+$ T cells secreted TNF- α , and these proportions were higher than those in the PBS, BCG, *IL-2*-rBCG and *BZLF1*-rBCG groups. Among these groups, *IL-2-BZLF1*-rBCG stimulated TNF- α secretion by $CD4^+$ T cells ($P = 0.0012$), and 3.65% and 0.28% of $CD8^+$ T cells secreted IFN- γ and TNF- α , respectively, compared with the PBS group. *IL-2-BZLF1*-rBCG stimulated greater secretion ($P = 0.0006$) of these cytokines than PBS, BCG, *IL-2*-rBCG, and *BZLF1*-rBCG, and it stimulated the secretion of TNF- α by $CD8^+$ T cells in a statistically significant manner (Fig. 5A, B, C, D).

After treatment with *IL-2-BZLF1*-rBCG, among splenic lymphocytes, 8.28% of $CD4^+$ T cells secreted IFN- γ , and 0.72% of $CD4^+$ T cells secreted TNF- α , which were higher than those in the PBS, BCG, *IL-2*-rBCG and *BZLF1*-rBCG groups. Additionally, 8.84% of $CD8^+$ T cells secreted IFN- γ , and 0.20% of $CD8^+$ T cells secreted TNF- α , which were higher than those in the PBS, BCG, *IL-2*-rBCG, and *BZLF1*-rBCG groups (Fig. 5E, F, G, H).

Flow cytometry analysis of cytokine secretion by rBCG-stimulated T cells

Splenic lymphocytes were isolated from rBCG-treated mice, further stimulated in vitro with different concentrations of

rBCG, and cultured for 48 h before flow cytometry analysis. The results showed that among the splenic lymphocytes stimulated with *IL-2-BZLF1*-rBCG at concentrations of 0/ml, 10^3 /ml and 10^6 /ml, 2.14%, 2.39% and 4.60% of $CD4^+$ T cells secreted IFN- γ , which were statistically significantly higher than those in the PBS, BCG, *IL-2*-rBCG and *BZLF1*-rBCG groups; 0.61%, 0.83% and 1.88% of $CD4^+$ T cells secreted TNF- α , which were statistically significantly higher than those in the PBS, BCG, *IL-2*-rBCG and *BZLF1*-rBCG groups, while 1.11%, 1.82% and 2.23% of $CD8^+$ T cells secreted IFN- γ , which were significantly higher than those in the PBS, BCG, *IL-2*-rBCG and *BZLF1*-rBCG groups. Moreover, 0.17%, 0.30% and 0.85% of $CD8^+$ T cells secreted TNF- α , which were significantly higher than those in the PBS, BCG, *IL-2*-rBCG and *BZLF1*-rBCG groups. Moreover, the proportion of $CD4^+$ T cells and $CD8^+$ T cells that secreted IFN- γ and TNF- α gradually increased with increasing rBCG concentration (Fig. 6).

CTLs

Splenic lymphocytes were isolated from mice that were treated with rBCG and cocultured with CNE-2Z nasopharyngeal carcinoma cells at ratios of 1:1, 2:1 and 4:1 for 24 h to measure the effect of splenic lymphocytes on killing CNE-2Z cells. The results showed that *IL-2-BZLF1*-rBCG-stimulated splenic lymphocytes killed

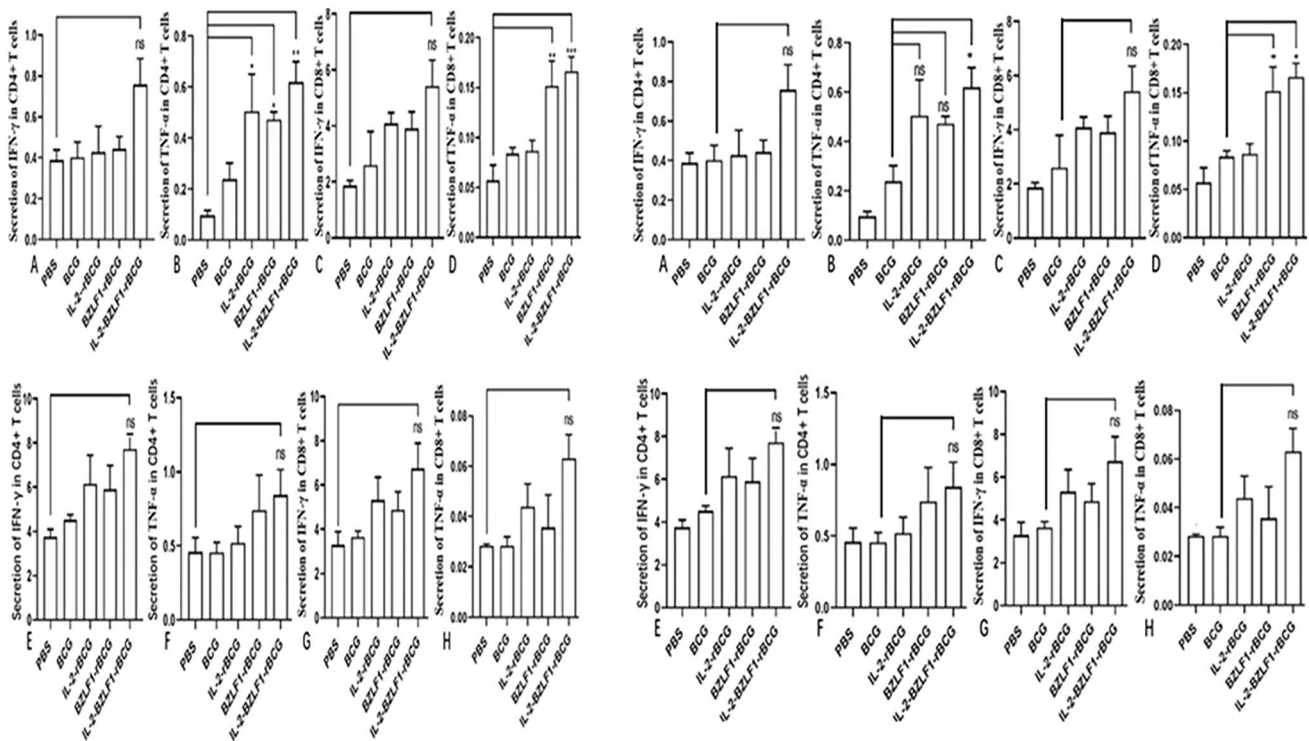


Fig. 5 Secretion of IFN- γ and TNF- α in blood and splenic CD4⁺ T cells and CD8⁺ T cells after different rBCG stimulations of the organism. **A** Secretion of IFN- γ in blood CD4⁺ T cells after different rBCG stimulations of the organism. A total of 1.21% of CD4⁺ T cells secreted IFN- γ , and these proportions were higher than those in the PBS (0.36%), BCG (0.45%), *IL-2-rBCG* (0.62%) and *BZLF1-rBCG* (0.64%) groups. **B** Secretion of TNF- α in blood CD4⁺ T cells after different rBCG stimulations of the organism. A total of 2.14% of CD4⁺ T cells secreted TNF- α , and these proportions were higher than those in the PBS (0.43%), BCG (0.60%), *IL-2-rBCG* (0.91%) and *BZLF1-rBCG* (0.87%) groups. **C** Secretion of IFN- γ in blood CD8⁺ T cells after different rBCG stimulations of the organism. Compared with those of the PBS group, 3.65% of CD8⁺ T cells secreted IFN- γ . *IL-2-BZLF1-rBCG* stimulated greater secretion ($P=0.0006$) of these cytokines than PBS (0.68%), BCG (1.30%), *IL-2-rBCG* (2.02%), and *BZLF1-rBCG* (2.63%). **D** Secretion of TNF- α in blood CD8⁺ T cells after different rBCG stimulations of the organism. A total of 0.28% of CD8⁺ T cells secreted TNF- α compared with that of the PBS group. *IL-2-BZLF1-rBCG* stimulated greater secretion ($P=0.0006$) of these cytokines than PBS (0.03%), BCG (0.10%), *IL-2-rBCG* (0.13%), and *BZLF1-rBCG* (0.13%), and it stimulated the secretion of TNF- α

by CD8⁺ T cells in a statistically significant manner. **E** Secretion of IFN- γ in splenic CD4⁺ T cells after different rBCG stimulation of the organism. A total of 8.28% of CD4⁺ T cells secreted IFN- γ , which was higher than that in the PBS (3.80%), BCG (4.19%), *IL-2-rBCG* (5.26%) and *BZLF1-rBCG* (4.47%) groups. **F** Secretion of TNF- α in splenic CD4⁺ T cells after different rBCG stimulation of the organism. After treatment with *IL-2-BZLF1-rBCG*, among splenic lymphocytes, 0.72% of CD4⁺ T cells secreted TNF- α , which was higher than that in the PBS (0.25%), BCG (0.44%), *IL-2-rBCG* (0.67%) and *BZLF1-rBCG* (0.88%) groups. Additionally, 0.20% of CD8⁺ T cells secreted TNF- α , which was higher than that in the PBS (0.04%), BCG (0.05%), *IL-2-rBCG* (0.14%), and *BZLF1-rBCG* (0.15%) groups. **G** Secretion of IFN- γ in splenic CD8⁺ T cells after different rBCG stimulation of the organism. Additionally, 8.84% of CD8⁺ T cells secreted IFN- γ , which was higher than that in the PBS (3.92%), BCG (4.82%), *IL-2-rBCG* (5.99%), and *BZLF1-rBCG* (5.58%) groups. **H** Secretion of TNF- α in splenic CD8⁺ T cells after different rBCG stimulation of the organism. Additionally, 0.20% of CD8⁺ T cells secreted TNF- α , which was higher than that in the PBS (0.04%), BCG (0.05%), *IL-2-rBCG* (0.14%), and *BZLF1-rBCG* (0.15%) groups

29.40%, 47.60% and 57.44% of total CNE-2Z cells, which was higher than that in the PBS (11.39%, 9.87%, and 11.45%), BCG (12.49%, 20.80%, and 30.09%), *IL-2-rBCG* (30.13%, 16.83%, and 26.11%) and *BZLF1-rBCG* (40.12%, 42.97%, and 53.19%) groups, with some statistical significance. Moreover, the killing of CNE-2Z cells gradually increased with increasing proportions of lymphocytes (Fig. 7). There were no significant differences between *BZLF1-rBCG* and *IL-2-BZLF1-rBCG*. Activation of CTLs mainly depends on the *BZLF1* protein.

Changes in tumor volume and weight in nude mice

Mice with nasopharyngeal carcinoma tumors were treated with rBCG injection, the tumors were measured every three days, and the changes in tumor volume were determined, as shown in Fig. 8A. Compared with the PBS, BCG, *IL-2-rBCG* and *BZLF1-rBCG* treatments, *IL-2-BZLF1-rBCG* injection resulted in a more effective reduction in tumor volume. The tumors of the treated nude mice were harvested and weighed, and the tumor weights of the

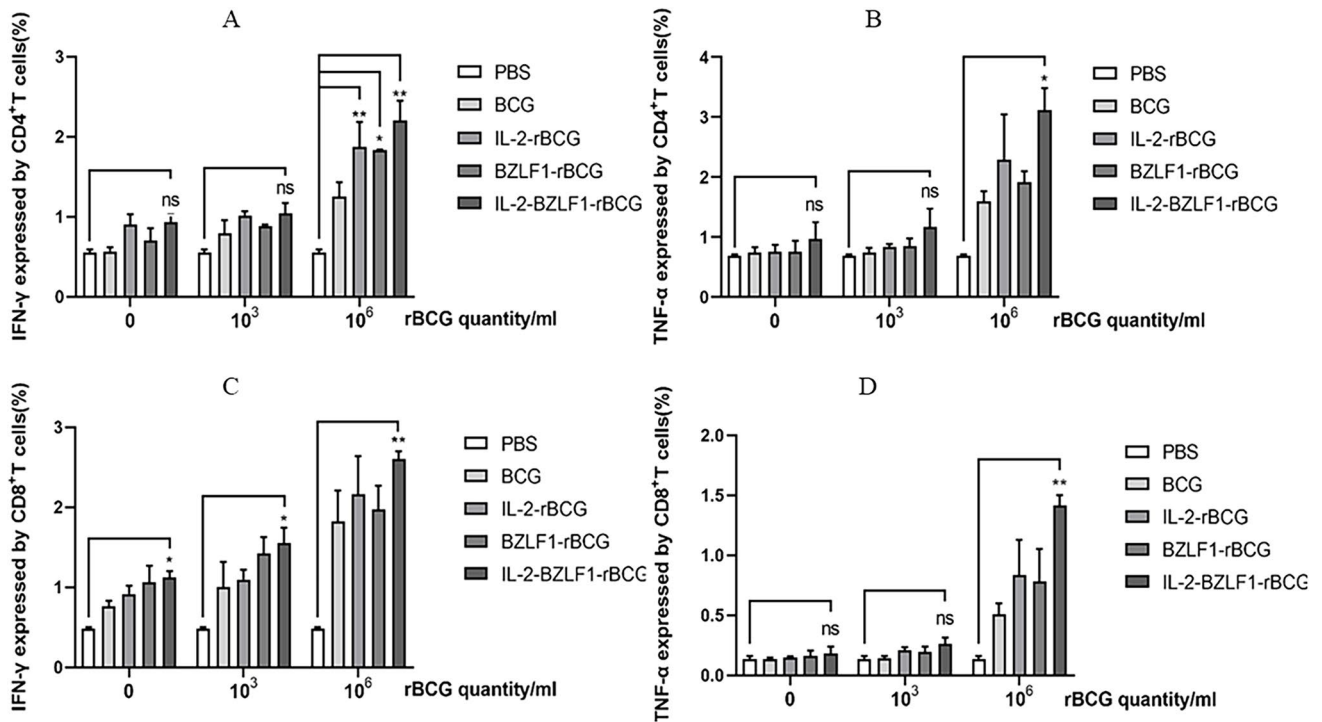


Fig. 6 Secretion of IFN- γ and TNF- α in CD4⁺ T cells and CD8⁺ T cells after stimulation of splenic lymphocytes with different concentrations of rBCG in vitro. **A** Secretion of IFN- γ in CD4⁺ T cells after stimulation of splenic lymphocytes with different concentrations of rBCG in vitro. The results showed that among the splenic lymphocytes stimulated with *IL-2-BZLF1*-rBCG at concentrations of 0/ml, 10³/ml and 10⁶/ml, 2.14%, 2.39% and 4.60% of CD4⁺ T cells secreted IFN- γ , respectively, which were significantly higher than those in the PBS (0.57%, 0.63%, and 0.69%), BCG (1.14%, 1.77%, and 2.65%), *IL-2*-rBCG (1.59%, 1.96%, and 3.21%) and *BZLF1*-rBCG (1.50%, 1.99%, and 3.50%) groups. **B** Secretion of TNF- α in CD4⁺ T cells after stimulation of splenic lymphocytes with different concentrations of rBCG in vitro. A total of 0.61%, 0.83% and 1.88% of CD4⁺ T cells secreted TNF- α , which were significantly higher than those in the PBS (0.2%, 0.18%, and 0.21%), BCG (0.28%, 0.38%, and 2.46%), *IL-2*-rBCG (0.30%, 0.46%, and 0.66%) and *BZLF1*-rBCG (0.32%,

0.55%, and 1.79%) groups. **C** Secretion of IFN- γ in CD8⁺ T cells after stimulation of splenic lymphocytes with different concentrations of rBCG in vitro. A total of 1.11%, 1.82% and 2.23% of CD8⁺ T cells secreted IFN- γ , which were significantly higher than those in the PBS (0.49%, 0.48%, and 0.51%), BCG (0.54%, 0.85%, and 1.38%), *IL-2*-rBCG (0.82%, 1.09%, and 1.48%) and *BZLF1*-rBCG (0.84%, 1.42% and 2.12%) groups. Moreover, we detected 0.17% and 0.30% (**D**) secretion of TNF- α in CD8⁺ T cells after stimulation of splenic lymphocytes with different concentrations of rBCG in vitro. A total of 0.85% of CD8⁺ T cells secreted TNF- α , which was significantly higher than that in the PBS (0.13%, 0.12%, and 0.11%), BCG (0.11%, 0.16%, and 0.37%), *IL-2*-rBCG (0.11%, 0.22%, and 0.41%) and *BZLF1*-rBCG (0.15%, 0.24%, and 0.52%) groups. *: $P < 0.05$ compared with the PBS group, which is statistically significant. **: $P < 0.01$ compared with the PBS group, which is statistically significant

IL-2-BZLF1-rBCG-treated group were significantly lower than those of the other treatment groups (Fig. 8B, C).

Hematoxylin–eosin staining

Tumors from rBCG-treated nude mice were fixed with 4% paraformaldehyde and sent to Jinan Jinyu for HE staining. More lymphocytes were observed in the tumor sections of the *IL-2-BZLF1*-rBCG-treated group (Fig. 8D, E, F).

Flow cytometry analysis of splenic NK cells

Spleens were harvested from rBCG-treated nude mice, and the percentage of NK cells was analyzed by flow cytometry. The results showed that NK cells in the *IL-2-BZLF1*-rBCG

treatment group accounted for 2.99% of total splenic cells, and this proportion was higher than that in the PBS (0.68%) and BCG (1.89%) groups, and the difference was statistically significant ($P < 0.001$) (Fig. 9).

Discussion

EBV, which is the only pathogen that can directly transform host B cells in vitro, has a strong ability to induce tumor formation, including including nasopharyngeal carcinoma, Burkitt's lymphoma tumors, Hodgkin's lymphoma cancer, gastric cancer, etc. (Kanda et al. 2019); however, there are no methods for the precise treatment and prevention of EBV infection (Chen et al. 2005). In recent years, researchers have

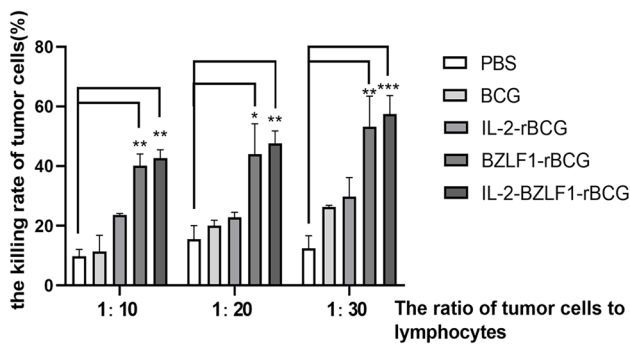


Fig. 7 In vitro killing of EBV-positive nasopharyngeal carcinoma tumor cells by splenic lymphocytes. Note: *: $P < 0.05$ compared with the PBS group, which is statistically significant; **: $P < 0.01$ compared with the PBS group, which is statistically significant; ***: $P < 0.001$ compared with the PBS group, which is statistically significant

conducted studies on recombinant EBV envelope protein vaccines, virus particle-like EBV vaccines, therapeutic EBV vaccines, and synthetic mRNA EBV vaccines (Kanda et al. 2019; Bernaudat et al. 2022) in an effort to identify a vaccine that can effectively prevent EBV-associated tumor formation. However, no vaccine has been shown to be effective in

preventing and treating EBV infection or EBV-associated tumor formation. In this study, we also attempted to generate an EBV vaccine. We ligated the human *IL-2* gene and the EBV *BZLF1* gene to form an *IL-2-BZLF1* fusion gene by a peptide splice $(Gly_4Ser)_3$ DNA sequence, and we ligated this fusion gene with the *E. coli-Mycobacterium tuberculosis* shuttle expression vector pMV261 by enzymatic cleavage. The recombinant plasmid *IL-2-BZLF1*-pMV261 was introduced into BCG to generate *IL-2-BZLF1*-rBCG. We hypothesized that rGCG can play a dual role in *IL-2* and *BZLF1* and that BCG can also activate the body's immune system. BCG has been used in the treatment of renal cell carcinoma, lymphoma and melanoma, and it has several advantages. (1) BCG is the most widely used vaccine in the world; it has been used in more than 3 billion people, and it has a strong safety profile; (2) BCG can simultaneously express multiple antigens from different pathogens; (3) BCG can be administered at any time after birth, and the effect of BCG is not affected by maternal antibodies; (4) BCG acts as an effective adjuvant to induce sustained antigenic stimulation and activate innate and adaptive immune responses; and (5) BCG is heat stable and inexpensive to produce (Abdallah and Behr 2017; Stover et al. 1991). By measuring the gene expression of *IL-2-BZLF1*-rBCG by real-time fluorescence

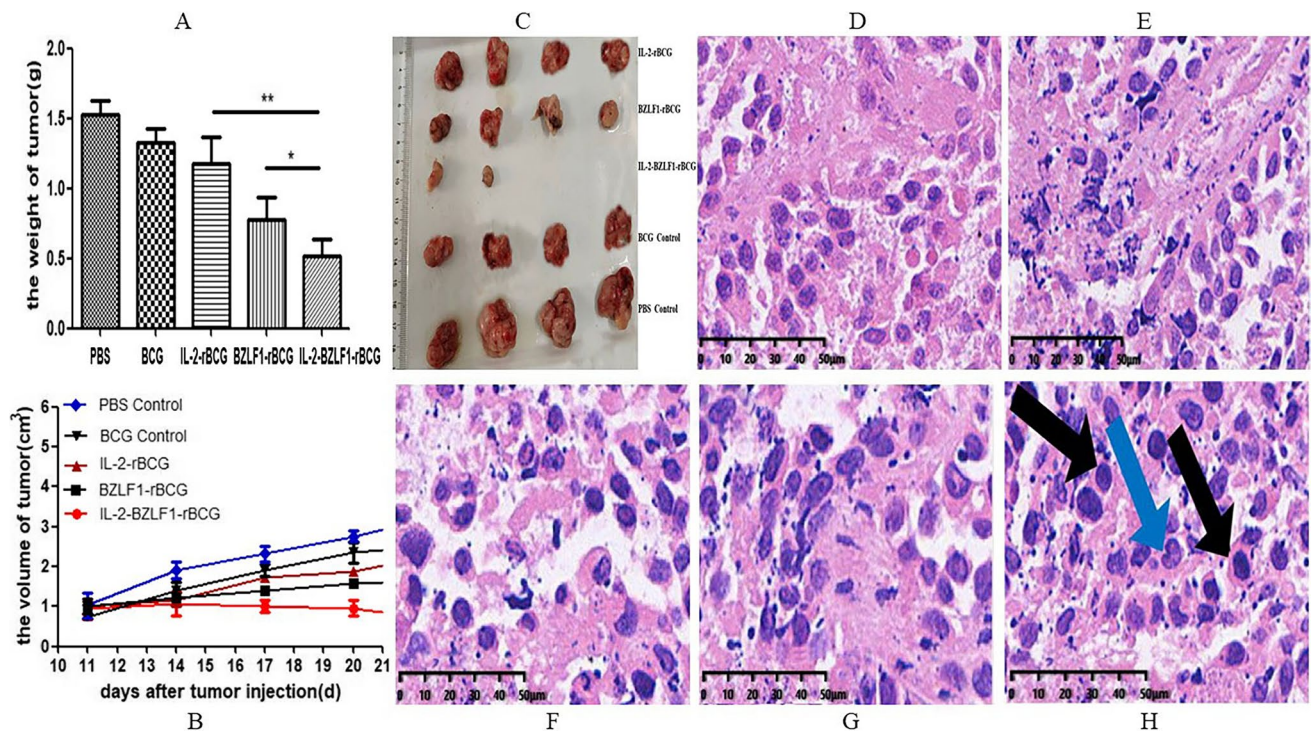


Fig. 8 Changes in tumors after different rBCG treatments in tumor-bearing nude mice. **A** Changes in tumor weight after different rBCG treatments in tumor-bearing nude mice. **B** Tumor volume after rBCG treatments in tumor-bearing nude mice, **: $P < 0.01$ compared with the BCG group, which is statistically significant. **C** Comparison of

tumor size in nude mice. **D** Tumor HE staining results after treatment with PBS. **E** Tumor HE staining results after treatment with BCG. **F** Tumor HE staining results after treatment with *IL-2-BZLF1*-rBCG (black arrows are lymphocytes, and blue arrows are mononuclear phagocytes)

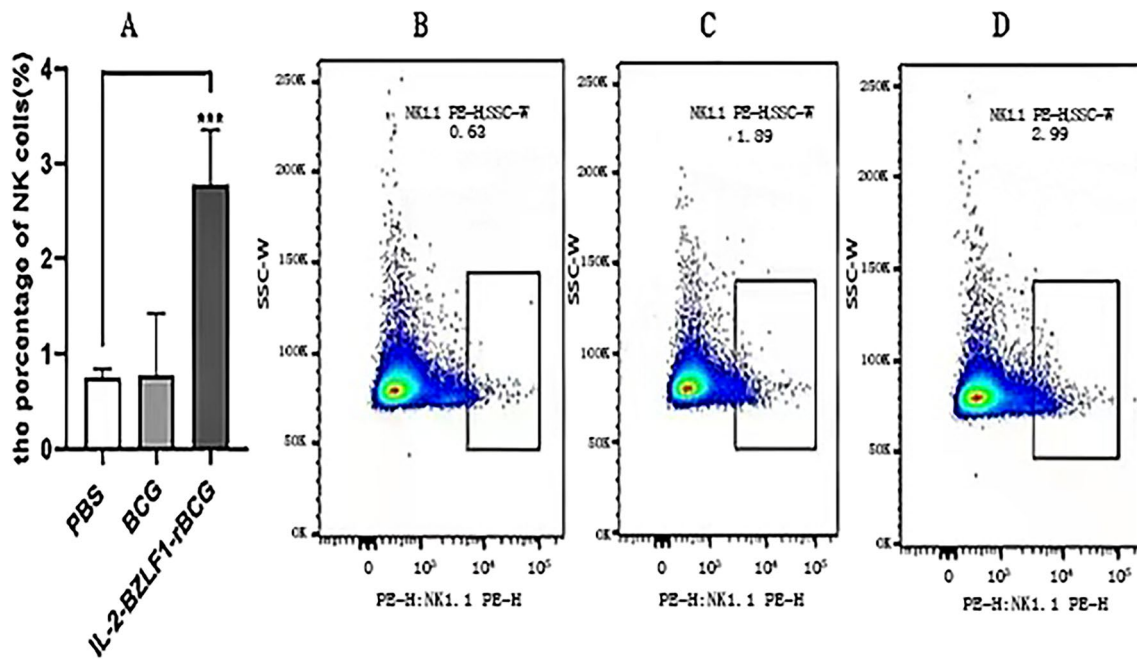


Fig. 9 Secretion of splenic NK cells after treatment with different rBCGs. Note: ***: $P < 0.001$ compared to the PBS group, which is statistically significant

quantitative PCR and Western blotting, we were able to confirm that *IL-2-BZLF1*-rBCG stably expresses both the IL-2 and BZLF1 proteins, laying the foundation for subsequent immune and therapeutic experiments in animals. Whether rBCG can replicate in the body is the key to its long-term existence. If recombinant BCG can exist for a long time, it will work for a long time. To date, there is no effective vaccine for the prevention of Epstein–Barr virus (EBV) infection, and our recombinant BCG will be the first of its kind.

CD4⁺ T and CD8⁺ T cells are the primary protective immune cells after EBV infection. The strong immunogenicity of rBCG-expressed BZLF1 induces immune responses in CD4⁺ T and CD8⁺ T cells (Raker et al. 2020). CD8⁺ T cells differentiate into cytotoxic T cells (CTLs), which are activated by T-cell receptors (TCRs) that recognize the combination of a major histocompatibility complex (MHC) and tumor cell surface antigens and release perforin. CTLs are activated by T-cell receptors (TCRs) that recognize the combination of a major histocompatibility complex (MHC) with tumor cell surface antigens (Yan et al. 2020). Then, they release perforin and granzyme B to induce the apoptosis of target cells (Cui and Snapper 2021). The incidence of EBV-related tumor formation is greatly increased under conditions that suppress T-cell activation (Kanda et al. 2019). In this study, rBCG-specific lymphocytes were cocultured with tumor cells in vitro, and it was found that *IL-2-BZLF1*-rBCG-specific T lymphocytes exert stronger effects on lysing tumor cells; *IL-2*-rBCG- and *BZLF1*-rBCG-specific lymphocytes lysed tumor cells, but these effects

were not as great as those of *IL-2-BZLF1*-rBCG-specific lymphocytes, which killed with higher efficiency.

During infection with BZLF1-deficient EBV, CD8⁺ T cells expand only half as much as during EBV infection, indicating that a significant proportion of CD8⁺ T cells recognize antigens from the EBV lytic phase. CD8⁺ T cells mostly recognize proteins that are expressed in the early cleavage phase, whereas CD4⁺ T cells mainly recognize proteins that are expressed in the late cleavage phase (Kanda et al. 2019). CD8⁺ T cells, which are effector cells of protective immunity, exert immunoprotective effects by inducing IFN- γ secretion through the activation of the costimulatory receptor 2B4 (Yin et al. 2019). CD3⁺ CD4⁻ CD8⁻ T cells can induce the secretion of IFN- γ by activating the Fas/FasL pathway to initiate tumor cell apoptosis, thus inhibiting lymphoma growth; however, IFN- γ that is secreted by CD3⁺ CD4⁻ CD8⁻ T cells is also involved in antitumor immune responses (Kerr 2019). In contrast, IL-2, which is a T-cell growth factor, can further stimulate the proliferation and activation of various immune cells, such as CD4⁺ T cells or CD8⁺ T cells, via the induction of Zta to elicit a stronger immune response. The application of BZLF1 and IL-2 genes is appropriate and necessary and may be useful for EBV vaccine research.

Flow cytometric analysis showed that *IL-2-BZLF1*-rBCG stimulated the secretion of TNF- α and IFN- γ by CD4⁺ T cells or CD8⁺ T cells in the mice. TNF- α , which is a 51-kDa nonglycosylated, noncovalently linked homotrimeric protein, is mainly secreted by activated macrophages and T

cells; this precursor protein is cleaved by TNF- α convertase to produce the soluble TNF- α protein, which can bind to TNF receptor type 1 (TNFR1), which is expressed in most cells, and TNFR2, which is expressed by only some immune cells (Bernaumat et al. 2022) and exerts antitumor effects (Mizui 2019). It has been reported that TNF- α can induce the proliferation and differentiation of Tc9 cells, which are a subpopulation of CD8⁺ T cells, through TNFR2, and Tc9 cells exhibit longer persistence in vivo and can exert stronger cytotoxic effects against tumor cells (Cui and Snapper 2021). After 12 days of stimulation of EBV-infected peripheral blood mononuclear cells with Zta in vitro, 7.34% and 16.52% of CD4⁺ T cells and CD8⁺ T cells secreted IFN- γ , respectively, confirming that Zta is mainly recognized by CD8⁺ T cells and that stimulation with Zta for a short period does not result in significant changes in IFN- γ production (Cui and Snapper 2021).

Currently, treatment of EBV-related tumors includes tumor immunotherapy, such as peripatetic T-cell therapy, EBV-specific TCR-engineered T-cell therapy, EBV-specific chimeric antigen receptor T-cell therapy, and therapeutic EBV vaccines; all of these approaches have definite therapeutic effects, but the associated limitations should not be ignored (Yin et al. 2019). For example, the cost was too high for the patients to bear. In this study, we investigated the pharmacological effect of *IL-2-BZLF1*-rBCG on EBV-positive nasopharyngeal carcinoma tumors in nude mice. The predilection of this virus for human cells makes it less likely to survive in ordinary mice; therefore, we chose to establish a tumor model by subcutaneously injecting CNE-2Z tumor cells into thymus-deficient nude mice (Marques-Neto et al. 2021).

Based on the results of the antitumor experiments, *IL-2-BZLF1*-rBCG effectively cleared the tumor cells by inducing the proliferation of CD4⁺ T cells, CD8⁺ T cells and NK cells, activating specific and nonspecific immune responses in the mice. IL-2 and BZLF1, when expressed by rBCG, have been previously applied in studies on tumor therapy. Xue et al. (2022) conducted a study of the antitumor effects of *BZLF1-LMP2*-rBCG and confirmed that rBCG activates the cellular immunity of the body and exerts antitumor effects. It has been reported that EBV infection mainly elicits immunoprotective responses from CD8⁺ T cells, NK cells, NKT cells and γ &T cells (Kanda et al. 2019). NK cells can induce the apoptosis of tumor cells through granzyme B and perforin secretion (Kerr 2019) and kill tumor cells via the ADCC mechanism (Bernaumat et al. 2022). In addition, NK cells also play a role in the immune detection of tumors and can be used to determine the prognosis of tumors (Hartlage et al. 2015). In humanized mice infected with EBV, the numbers of NK cells are significantly increased, whereas in mouse models that lack NK cells, the EBV viral load is considerably higher and more likely to induce EBV-associated

tumor formation (Yin et al. 2019); these results also confirm the active role of NK cells in tumor control. NK cells stimulate the proliferation of dendritic cells, increase the production of proinflammatory factors, and elicit relevant immune responses (Mizui 2019; Shimasaki et al. 2020). Moreover, BCG can stimulate the production of IFN and TNF, enhance tumor immunogenicity in vivo and exert killing or inhibitory effects on tumor cells (Yan et al. 2020).

In this study, we constructed an *IL-2-BZLF1*-rBCG subunit vaccine and confirmed that *IL-2-BZLF1*-rBCG can exert antitumor effects by stimulating the immune system. This study lays the foundation for the treatment and prevention of EBV-related tumors through experiments related to tumor treatment.

Supplementary Information The online version contains supplementary material available at <https://doi.org/10.1007/s00253-023-12851-3>.

Acknowledgements The authors thank Shuang Wang and Yanlin Qu for their excellent technical assistance.

Author contributions QX, HX and YL designed the study. MY, TM, JL and LC conducted most of the experiments. QX and MY wrote the paper. QX, MY, TM and LC analyzed and interpreted the data. QX and YL revised the manuscript. All authors reviewed and approved the manuscript.

Funding This study was funded by the Shandong Medical and Health Technology Development Plan Project of Shandong Province (2017WS339), the Key Research and Development Plan project of Shandong (2018GCF118137), Innovation and Entrepreneurship Training Program for College Students of Shandong Province (S202110443029), the Research Fund for Lin He's Academician Workstation of New Medicine and Clinical Translation in Jining Medical University (JYHL2019ZD03), and the Science and Technology Project of Colleges in Shandong Province (J17KB085).

Data availability All data generated or analyzed during this study are included in this published article (and its additional files). Requests for material should be made to the corresponding authors.

Declarations

Ethics approval All procedures performed in studies involving mice were in accordance with the ethical standards of the institutional and national research committee and with the 1964 Helsinki Declaration and its later amendments or comparable ethical standards. All animal experiments were approved by the Shandong animal experimentation committees (2009–0023; approval date, 2/25/09–3/25/14).

Competing interests The authors declare no competing interests.

References

- Abdallah AM, Behr MA (2017) Evolution and strain variation in BCG. *Adv Exp Med Biol* 1019:155–169. https://doi.org/10.1007/978-3-319-64371-7_8
- Bernaumat F, Gustems M, Günther J, Oliva MF, Buschle A, Göbel C, Pagniez P, Lupo J, Signor L, Müller CW, Morand P, Sattler M, Hammerschmidt W, Petosa C (2022) Structural basis of DNA

- methylation-dependent site selectivity of the Epstein-Barr virus lytic switch protein ZEBRA/Zta/BZLF1. *Nucleic Acids Res* 50(1):490–511. <https://doi.org/10.1093/nar/gkab1183>
- Chen F, Liu C, Lindvall C, Xu D, Ernberg (2005) Epstein-Barr virus latent membrane ZA(LMP2A)down regulates telomerase reverse transcriptase(hTERT) in epithelial cell lines. *Int J Cancer* 113:284–289. <https://doi.org/10.1002/ijc.20594>
- Cui X, Snapper CM (2021) Epstein Barr virus: Development of vaccines and immune cell therapy for EBV-associated diseases. *Front Immunol* 12:734471. <https://doi.org/10.3389/fimmu.2021.734471>
- Hartlage AS, Liu T, Patton JT, Garman SL, Zhang XL, Kurt H, Lozanski G, Lustberg ME, Caligiuri MA, Baiocchi RA (2015) The Epstein-Barr virus lytic protein BZLF1 as a candidate target antigen for vaccine development. *Cancer Immunol Res* 3(7):787–794. <https://doi.org/10.1158/2326-6066.CIR-14-0242>
- Kanda T, Yajima M, Ikuta K (2019) Epstein-Barr virus strain variation and cancer. *Cancer Sci* 110(4):1132–1139. <https://doi.org/10.1111/cas.13954>
- Kerr JR (2019) Epstein-Barr virus (EBV) reactivation and therapeutic inhibitors. *J Clin Pathol* 72(10):651–658. <https://doi.org/10.1136/jclinpath-2019-205822>
- Marques-Neto LM, Piwowarska Z, Kanno AI, Moraes L, Trentini MM, Rodriguez D, Silva JLSC, Leite LCC (2021) Thirty years of recombinant BCG: new trends for a centenary vaccine. *Expert Rev Vaccines* 20(8):1001–1011. <https://doi.org/10.1080/14760584.2021.1951243>
- Mizui M (2019) Natural and modified IL-2 for the treatment of cancer and autoimmune diseases. *Clin Immunol* 206:63–70. <https://doi.org/10.1016/j.clim.2018.11.002>
- Raker VK, Becker C, Landfester K, Steinbrink K (2020) Targeted activation of T cells with IL-2-coupled nanoparticles. *Cells* 9(9):2063. <https://doi.org/10.3390/cells9092063>
- Rist MJ, Neller MA, Burrows JM, Burrows SR (2015) T-cell epitope clustering in the highly immunogenic BZLF1 antigen of Epstein-Barr virus. *J Virol* 89(1):703–712. <https://doi.org/10.1128/JVI.02642-14>
- Salomon BL, Leclerc M, Tosello J, Ronin E, Piaggio E, Cohen JL (2018) Tumor necrosis factor α and regulatory T cells in oncoimmunology. *Front Immunol* 9:444. <https://doi.org/10.3389/fimmu.2018.00444>
- Shimasaki N, Jain A, Campana D (2020) NK cells for cancer immunotherapy. *Nat Rev Drug Discov* 19(3):200–218. <https://doi.org/10.1038/s41573-019-0052-1>
- Stover CK, Dela Cruz VF, Fuerst TR, Burlein JE, Benson LA, Bennett LT, Bansal GP, Young JF, Lee MH, Hatfull GF, Snapper SB, Barletta RG, Jacobs WR Jr, Bloom BR (1991) New use of BCG for recombinant vaccines. *Nature* 351(6326):456–460. <https://doi.org/10.1038/351456a0>
- Treuer R, Haydel SE (2011) Acid-fast staining and petroff hausser chamber counting of mycobacterial cells in liquid suspension. *Curr Protoc Microbiol*: 1–8. <https://doi.org/10.1002/9780471729259.mc10a06s20>
- Xue QJ, Yu HX, Liu A, Wang H, Chen T, Li YQ, Chen T, Wang QL (2022) The inhibitory effect of rBCG on EB virus-positive tumors using an EB virus fusion gene. *Appl Microbiol Biotechnol* 106(1):185–195. <https://doi.org/10.1007/s00253-021-11682-4>
- Yan YC, Xue QJ, Liu A, Li XZ, Yang YY, Chen T, Li SG (2020) EB virus-positive tumors are inhibited by rBCG expressing hGM-CSF and LMP2A. *Hum Vaccin Immunother* 16(3):654–663. <https://doi.org/10.1080/21645515.2019.1670593>
- Yin H, Qu J, Peng Q, Gan R (2019) Molecular mechanisms of EBV-driven cell cycle progression and oncogenesis. *Med Microbiol Immunol* 208(5):573–583. <https://doi.org/10.1007/s00430-018-0570-1>

Publisher's Note Springer Nature remains neutral with regard to jurisdictional claims in published maps and institutional affiliations.

Springer Nature or its licensor (e.g. a society or other partner) holds exclusive rights to this article under a publishing agreement with the author(s) or other rightsholder(s); author self-archiving of the accepted manuscript version of this article is solely governed by the terms of such publishing agreement and applicable law.